Plasma Sci. Technol. **24** (2022) 124002 (10pp) https://doi.org/10.1088/2058-6272/ac9f2e

Study of the spectrum effect on the threshold of resonant magnetic perturbation penetration on J-TEXT

Feiyue MAO (毛飞越)[1], **Nengchao WANG** (王能超)[1,*], **Zhuo HUANG** (黄卓)[2], **Zhengkang REN** (任正康)[1], **Song ZHOU** (周松)[1], **Chengshuo SHEN** (沈呈硕)[1], **Xiaoyi ZHANG** (张霄翼)[1], **Ying HE** (何莹)[1], **Qi ZHANG** (张琪)[1], **Ruo JIA** (贾若)[1], **Chuanxu ZHAO** (赵传旭)[1], **Yangbo LI** (李杨波)[1], **Bo HU** (胡博)[1], **Da LI** (李达)[1], **Abba Alhaji BALA**[1,3], **Zhipeng CHEN** (陈志鹏)[1], **Zhongyong CHEN** (陈忠勇)[1], **Zhoujun YANG** (杨州军)[1], **Yunfeng LIANG** (梁云峰)[1,4,5], **Yonghua DING** (丁永华)[1], **Yuan PAN** (潘垣)[1] **and the J-TEXT Team**[1,6]

[1] International Joint Research Laboratory of Magnetic Confinement Fusion and Plasma Physics, State Key Laboratory of Advanced Electromagnetic Engineering and Technology, School of Electrical and Electronic Engineering, Huazhong University of Science and Technology, Wuhan 430074, People's Republic of China
[2] College of Computer Science, South-Central Minzu University, Wuhan 430074, People's Republic of China
[3] Physics Department, Federal University Dutse, Dutse 720101, Jigawa, Nigeria
[4] Forschungszentrum Jülich GmbH, Institut für Energie- und Klimaforschung–Plasmaphysik, Partner of the Trilateral Euregio Cluster (TEC), Jülich 52425, Germany
[5] Institute of Plasma Physics, Chinese Academy of Sciences, Hefei 230031, People's Republic of China

E-mail: wangnc@hust.edu.cn

Received 15 August 2022, revised 31 October 2022
Accepted for publication 1 November 2022
Published 29 November 2022

Abstract

The spectrum effect on the penetration of resonant magnetic perturbation (RMP) is studied with upgraded in-vessel RMP coils on J-TEXT. The poloidal spectrum of the RMP field, especially the amplitudes of $2/1$ and $3/1$ components, can be varied by the phase difference between the upper and lower coil rows, $\Delta\phi = \phi_{\rm top} - \phi_{\rm bottom}$, where $\phi_{\rm top}$ and $\phi_{\rm bottom}$ are the toroidal phases of the $n = 1$ field of each coil row. The type of RMP penetration is found to be related to $\Delta\phi$, including the RMP penetration of either $2/1$ or $3/1$ RMP and the successive penetrations of $3/1$ RMP followed by the $2/1$ RMP. For cases with penetration of only one RMP component, the penetration thresholds measured by the corresponding resonant component are close for various $\Delta\phi$. However, the $2/1$ RMP penetration threshold is significantly reduced if the $3/1$ locked island is formed in advance. The changes in the rotation profile due to $3/1$ locked island formation could partially contribute to the reduction of the $2/1$ thresholds.

Keywords: tokamak, error field, resonant magnetic perturbation, mode penetration, spectrum analysis

(Some figures may appear in colour only in the online journal)

1. Introduction

Tokamaks confine plasmas with their dominantly axisymmetric magnetic fields. However, there are still asymmetric fields called three-dimensional magnetic perturbations (MPs). MPs arise from imperfect coil fabrications called intrinsic error fields (IEFs) [1], saddle or helical coils [1, 2] and even magnetohydrodynamic (MHD) modes [3]. These small asymmetric fields can have great effects on plasma performance. For example, MPs can excite the locked mode (LM) and lead to the degradation of confinement and even disruption [2]. On the other hand, MPs can be used or

* Author to whom any correspondence should be addressed.
[6] See N Wang *et al* 2022 Advances in physics and applications of 3D magnetic perturbations on the J-TEXT tokamak, *Nucl. Fusion* 62 042016.

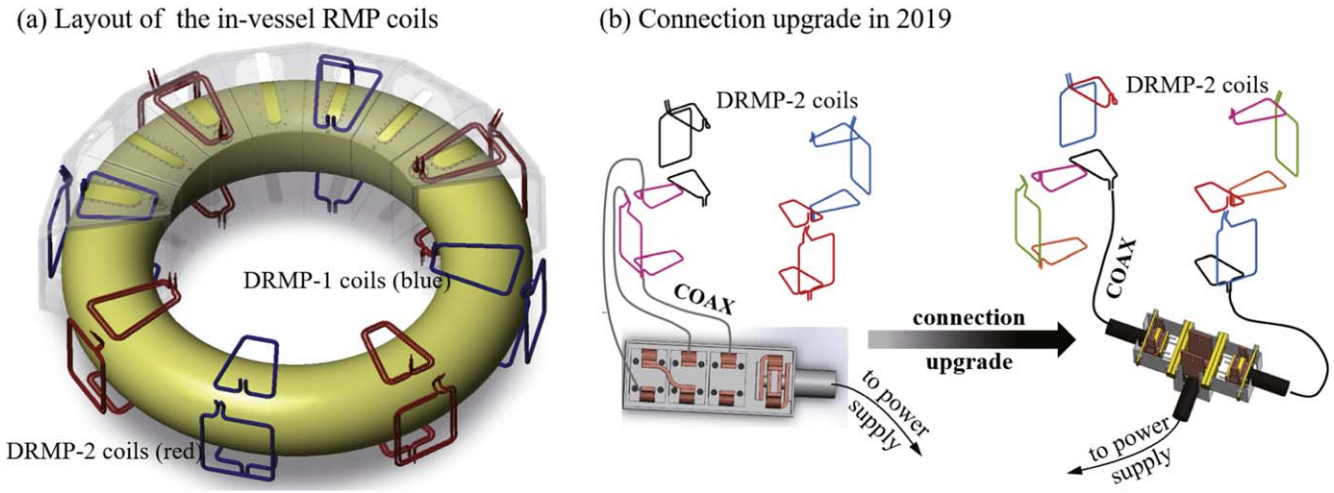

Figure 1. (a) The in-vessel RMP coils on J-TEXT, consisting of DRMP-1 coils (blue) and DRMP-2 coils (red) [28]. Reproduced from [28]. © 2019 IAEA, Vienna. CC BY 3.0. The yellow torus represents the plasma. (b) Diagram of the DRMP-2 coil connection upgrade.

optimized to control MHD instabilities such as the resistive wall mode (RWM) [4] and edge-localized mode (ELM) [5–7]. Mode penetrations (or field penetrations), which are known as forced magnetic reconnection [8] at the resonant surface (RS) in a tokamak plasma, are observed to be highly involved in LM formation [2] and ELM suppression [9–11]. Hence, the study of mode penetration is very important for device operation.

Multiple external saddle coils are available and common for IEF correction and ELM suppression in tokamaks [12–15]. The poloidal Fourier component distribution (also called poloidal spectrum) of MPs, which is determined by the saddle coil configuration, plays a crucial role in IEF correction and ELM control [16–20]. The ultimate goal of MP spectrum research is to find a perfect external coil configuration that suppresses ELMs without bad effects on plasma performance [20–22]. The effects of the MP spectrum on these issues contain the following aspects. First, the MP spectra of saddle coils are wide band. Resonant and non-resonant components are contained, resulting in multiple plasma responses. Second, owing to the complicated plasma responses, more than one component in the MP spectrum plays a part in mode penetration [16, 23, 24]. Third, non-resonant effects such as neoclassical toroidal viscosity (NTV) could affect the mode penetration by changing plasma rotation [25, 26]. Moreover, mode coupling and interactions between resonant surfaces should also be considered. A mode could be destabilized by another mode [27].

J-TEXT is a medium size tokamak equipped with 24 in-vessel saddle coils [28]. Based on these coils, mode penetrations and threshold scaling have been widely studied [29–32]. Recently, an upgrade on RMP coil connection was made to enable spectral modulation on J-TEXT, making it possible to study the spectrum effect on mode penetration. Mode penetrations are achieved with different MP spectra. Multiple mode penetration and the effects during a discharge were studied. The rest of this paper is organized as follows. In section 2, the experimental setup and RMP coil configurations are presented. The typical phenomena, thresholds and IEFs of $2/1$ and $3/1$ mode penetrations are presented in section 3. The phenomena and effects of multiple mode penetrations will be introduced in section 4. In section 5, a simple discussion on the reduction of the $2/1$ mode penetration thresholds is given. Finally, a summary is provided in section 6.

2. Experimental setup and RMP coil configuration

The J-TEXT tokamak is a conventional iron core tokamak with a major radius $R_0 = 105$ cm and a minor radius $a = 25$–29 cm [28]. J-TEXT usually operates in two configurations: the limiter configuration and the poloidal divertor configuration with an X-point on the high-field side. The current auxiliary heating on J-TEXT is the 105 GHz/500 kW electron cyclotron resonance heating system [33]. In this work, the plasma is operated on an ohmically heated limiter configuration. The plasma parameters are set to have a minor radius of 25.5 cm, a toroidal field of 1.7 T, a plasma current of 160 kA and an edge safety factor of 3.3.

The RMP coils on J-TEXT consist of 24 in-vessel saddle coils, half of which are in single-turn [34] with the others being double [28, 35], named DRMP-1 and DRMP-2. Figure 1 shows (a) the layout of the in-vessel RMP coils on J-TEXT [28] and (b) the diagram of the connection between coils. Initially, the connections of the top, low-field side and bottom coils at the same toroidal phase were fixed, such as in the experiments carried out in [30–32]. With this connection, a rotational RMP cam be conveniently achieved but the poloidal spectrum of the MP field will be hard to adjust. In 2019, the connections of DRMP-2 coils were changed from poloidal connections of three coils on the same toroidal location to toroidal connections of the same poloidal location but opposite toroidal locations, making the double-turn coils into six groups. The two coils in each group are fed current

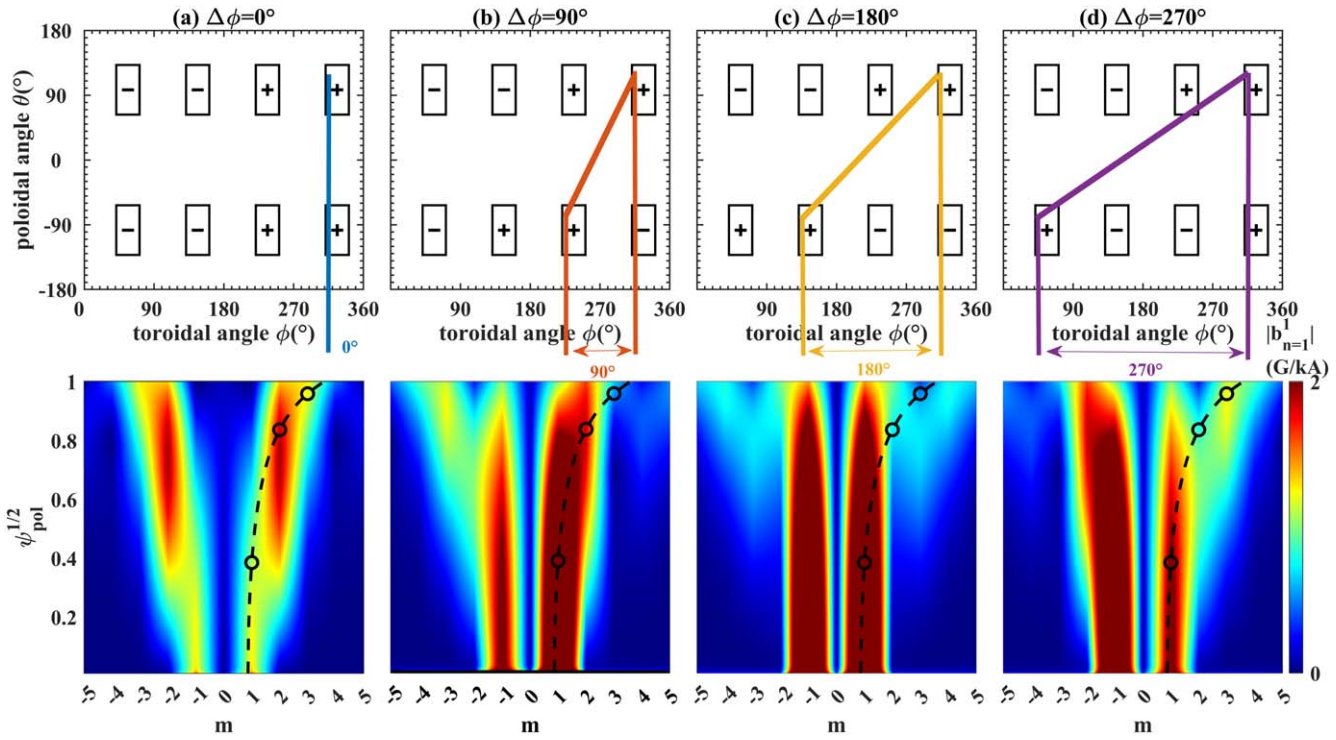

Figure 2. DRMP-2 coil configurations (upper) and corresponding spectra (lower) in four typical phase differences $\Delta\phi$: (a) 0°, (b) 90°, (c) 180°, (d) 270°. The dashed lines with open circles represent the rational surfaces.

with either the opposite or the same direction to produce MP field with toroidal number n being odd or even, respectively. By controlling the current ratio in the two group at the same row, the toroidal phase (ϕ_{top}, ϕ_{middle}, ϕ_{bottom},) of $n = 1$ MP can be set at any value from 0° to 360°. With the new connection, the poloidal spectrum of MP can be adjusted easily. Further details about this spectral adjustment are shown in [36]. In this work, the top and bottom coils of DRMP-2 are used to adjust the poloidal spectrum by coil phasing. Figure 2 shows the typical coil configurations of four different coil phasings. By feeding appropriate current in the coils, the phase difference between the upper and lower coil rows, $\Delta\phi = \phi_{\text{top}} - \phi_{\text{bottom}}$, where ϕ_{top} and ϕ_{bottom} are the toroidal phases of $n = 1$ field of each coil rows, can be set at any value from 0° to 360° and then the poloidal spectrum varies.

The RMP penetrations can be confirmed and distinguished in several aspects with various diagnostics on J-TEXT [30, 31, 37]. Here we show the diagnostics used in the RMP penetration experiments. The multichannel polarimeter-interferometer (POLARIS) [38] is used for electron density (n_e) measurement. The electron temperature (T_e) is measured by a multichannel electron cyclotron emission (ECE) radiometer [39]. A spectrometer filtered for carbon V viewing the plasma in the toroidal direction is used to give the toroidal velocity of plasma rotation (V_ϕ) [40]. Magnetic perturbations including static and oscillating perturbations are detected by the MHD magnetic diagnostic on J-TEXT [41]. Details of these measurements during mode penetrations are presented in section 3.

3. Typical phenomena of RMP penetrations and thresholds

Despite only a few coils being used, RMP penetration occurs in all of the phase differences $\Delta\phi$ with the plasma parameters mentioned above and core line-average electron density $n_e \sim 1 \times 10^{19}\,\text{m}^{-3}$. Table 1 shows the $m/n = 2/1$ and $3/1$ RMP components at the corresponding RS calculated with the vacuum assumption and the results of RMP penetration with varying $\Delta\phi$. The positions of RSs are given by the equilibrium and fitting code (EFIT) [42], $r_{q=2} \approx 19\,\text{cm} \approx 0.74a$, $r_{q=3} \approx 23\,\text{cm} \approx 0.9a$ (a is the minor radius). It can be found that the type of RMP penetration depends on $\Delta\phi$. RMP penetrations of $m/n = 2/1$ [30] and $3/1$ [31] have been reported on J-TEXT. Various phenomena related to locked islands are helpful to confirm and distinguish RMP penetrations [37, 39, 43, 44]. The details of the $2/1$ and $3/1$ RMP penetrations are as follows.

3.1. m/n = 2/1 RMP penetration and thresholds at various poloidal spectra

Figure 3 shows the time evolution of a discharge with $2/1$ RMP penetration. The RMP coil current (blue line in figure 3(a)) is programmed to ramp up slowly in a tearing stable plasma. In this discharge, the phase difference $\Delta\phi$ is set as 30°, so the applied RMP field has a dominant $2/1$ component. The radial field ($b_r^{n=1}$, red line in figure 3(a)) measured by magnetic probes in the high-field side (HFS) midplane increases linearly with the coil current (I_{coil})

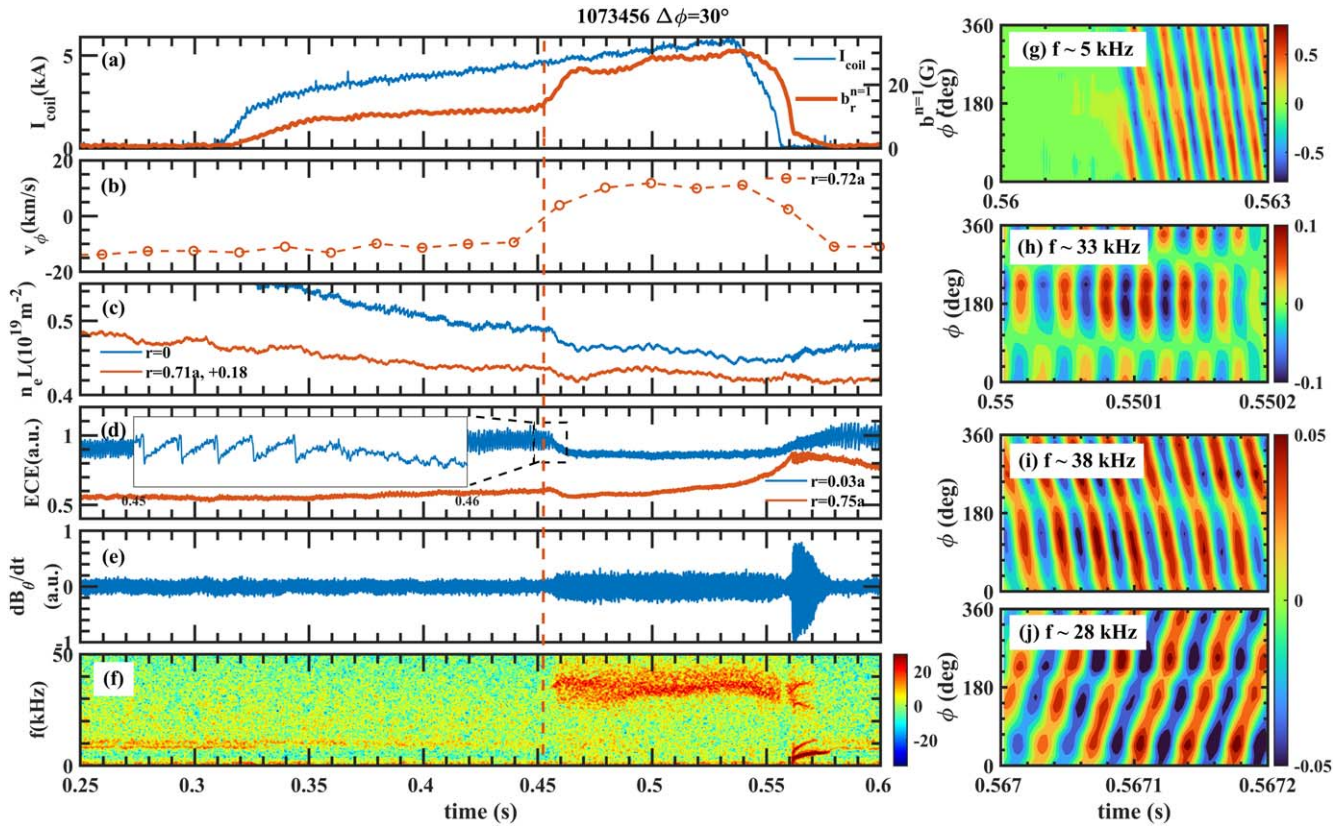

Figure 3. Time evolution of plasma parameters during 2/1 RMP penetration discharge #1073456 with (a) RMP coil current and the measured $n = 1$ radial magnetic field, (b) toroidal rotation (co-I_p is the positive direction), (c) line integrated electron density at the plasma core and around the 2/1 RS, (d) ECE signals around the core and the 2/1 RS, (e) Mirnov signal, (f) spectrogram of the Mirnov signal, (g)–(j) the contour plots of filtered signals measured by toroidal Mirnov probes.

Table 1. Results of mode penetration with $\Delta\phi$ scanning.

$\Delta\phi$ (°)	$b^{\rho}_{2/1}$ (G kA^{-1})	$b^{\rho}_{3/1}$ (G kA^{-1})	2/1 RMP penetration	3/1 RMP penetration
0	1.42	0.94	√	×
30	1.46	0.73	√	×
60	1.39	0.46	√	×
90	1.24	0.16	√	×
120	0.99	0.15	√	×
150	0.68	0.45	×	√
180	0.33	0.72	×	√
210	0.05	0.93	×	√
240	0.43	1.09	√	√
270	0.77	1.17	√	√
300	1.07	1.17	√	√
330	1.29	1.10	√	√

because of the linear plasma response and the pick-up field from RMP coils. The coefficient and phase of this $n = 1$ linear response depend on $\Delta\phi$. A detailed study on the linear response is not the topic of this work and it will be presented in the future. When the coil current reaches a critical value, a bifurcation occurs. The moment of this bifurcation is marked by the red vertical dashed line. There is a sudden increase in $b_r^{n=1}$ which indicates that a locked island is stimulated simultaneously. The plasma rotation around the 2/1 RS is changed towards co-I_p direction (co-I_p is the positive direction) and changed to approximately 15 km s^{-1} during the 2/1 RMP penetration in figure 3(b). According to a previous study of plasma rotation and tearing mode on J-TEXT [44], the plasma rotation in the toroidal direction is about 15 km s^{-1} when the 2/1 tearing island is stationary. These variations in radial magnetic field and plasma rotation provide strong evidence for 2/1 RMP penetration.

Figures 3(c) and (d) show the line integrated density n_eL and electron temperature T_e of the core and around 2/1 RS. The line integrated density n_eL around 2/1 RS has 0.18×10^{19} m^{-2} added for a better presentation. The decreasing tendency of density in this discharge is due to insufficient gas puffing. These signals drop significantly after 2/1 mode penetration. Meanwhile, the sawtooth oscillations in the core ECE signal disappear after mode penetration. These phenomena indicate a substantial degradation of plasma confinement.

Figures 3(e) and (f) show one channel of the Mirnov probes and its time–frequency spectrum. The waveform of the Mirnov signal (db_θ/dt) can be divided into three different states: no island state before 0.46 s, locked island state from 0.46 to 0.561 s, rotating island and fading stage after 0.561 s. During the rotating island stage, the oscillation on the Mirnov signal increases suddenly. A mode with an increasing

frequency from zero to several kilohertz arises on the spectrogram. These Mirnov signal and spectrogram phenomena indicate that the island unlocks and spins up. The contour plot (g) is from the signals of the toroidal Mirnov probe array and is filtered with a frequency range lower than 10 kHz. The contour plot (g) shows that the island unlocks and propagates in the counter-I_p direction with several kilohertz. There is a frequency of approximately 30–40 kHz during locked island stage. This mode splits into two branches with a higher frequency f_H and a lower frequency f_L. According to previous studies [37, 43, 45, 46], this mode is recognized as a beta-induced Alfvén eigenmode (BAE). Due to the strong correlation with the magnetic island, this mode is named m-BAE. It has the following features: the existence of the m-BAE is always related to the magnetic island; the m-BAE has two branches that propagate in opposite directions in the island frame and form a standing wave in the island frame; the frequencies of the m-BAE and the island have the relationship $f_H - f_{TM} = f_{TM} - f_L$ ($f_{TM} = +5$ kHz, $f_H = +38$ kHz, $f_L = -28$ kHz in the rotating island phase here). When the island is stationary, the two branches show a standing wave structure in the lab frame. Figure 3(h) show the standing wave structure during the locked island stage. Figures 3(i) and (j) show the traveling wave structures that propagate in opposite directions during the rotating island stage.

In every single discharge, the RMP coil current and plasma density at the moment of penetration are recorded for the database of penetration thresholds. The threshold $b^{\rho}_{2/1,\mathrm{th}}$ can be obtained from the RMP coil current threshold and RMP spectrum. Figure 4 shows the statistical results of the 2/1 RMP penetration thresholds over a wide density range. All of these data points share the same plasma parameters except electron density. Several sets of data are presented with different RMP spectra, i.e. $\Delta\phi = 0°$, 90° and others. In figure 4, the thresholds of $\Delta\phi = 0°$ and $\Delta\phi = 90°$ are marked by blue circles and red squares. Red crosses represent the maximum values of RMP when it failed to achieve mode penetration. For $\Delta\phi = 0°$, the threshold of 2/1 RMP penetration shows a non-monotonic dependence on the core line-average electron density, which shows the same regularity as in [32] for another spectrum. The non-monotonic dependence is explained because the plasma toroidal rotation varies non-monotonically with increasing density [32]. For another spectrum of $\Delta\phi = 90°$, the threshold of 2/1 RMP penetration is very close to the threshold of $\Delta\phi = 0°$ at the lower density range ($n_e < 1.3 \times 10^{19}\ \mathrm{m}^{-3}$). When the density is over $1.3 \times 10^{19}\ \mathrm{m}^{-3}$, the RMP failed to penetrate at $\Delta\phi = 90°$. The maximum value of the 2/1 RMP component for $\Delta\phi = 0°$ is 9 G, which is lower than the threshold of $\Delta\phi = 90°$ in a higher density range ($n_e > 1.3 \times 10^{19}\ \mathrm{m}^{-3}$). Three more discharges with other values of $\Delta\phi$ (30°, 60°, 120°) also show 2/1 RMP penetration, with the thresholds being marked by the yellow diamonds in figure 4. The thresholds at these $\Delta\phi$ are also close to the thresholds of $\Delta\phi = 0°$. These sets of data with different spectra indicate that the 2/1 RMP penetration threshold can be described by the vacuum 2/1 RMP component and the poloidal spectrum has few effects on the threshold in these situations.

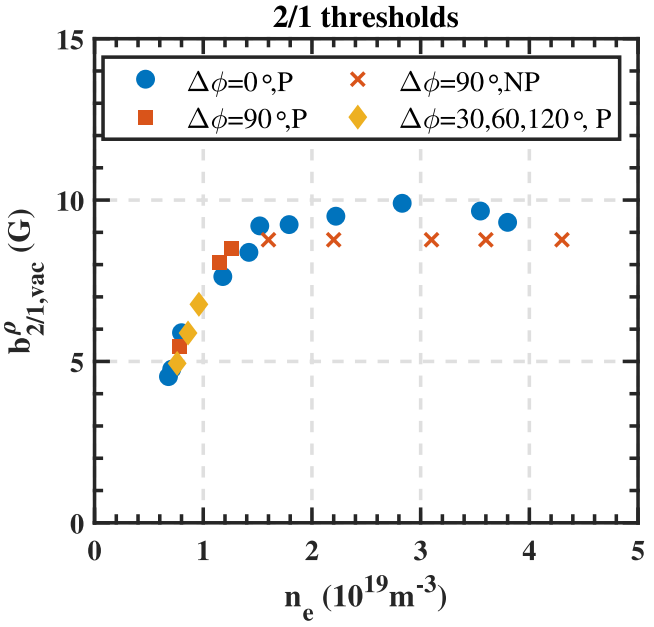

Figure 4. 2/1 RMP penetration thresholds obtained at various electron densities for several $\Delta\phi$ cases. The blue circles (●) represent thresholds with $\Delta\phi = 0°$, the red squares (■) represent thresholds with $\Delta\phi = 90°$ and the red crosses (×) represent the no penetration cases even at the maximal current with $\Delta\phi = 90°$. The yellow diamonds (♦) represent thresholds of discharges with $\Delta\phi = 30°$, 60°, 120°.

3.2. m/n = 3/1 RMP penetration and thresholds at various poloidal spectra

Compared with 2/1 RMP penetration, the signal changes due to 3/1 RMP penetration are weaker and need careful confirmation. Figure 5 presents typical signals during 3/1 RMP penetration with $\Delta\phi = 210°$, which has a 3/1 dominant RMP. The RMP coil current is ramped up to a maximum of 6 kA, and hence produces a maximum 3/1 RMP field at 5.6 G. During the early ramp-up phase of RMP, the pick-up field and plasma response measured by $b_r^{n=1}$ increases linearly with I_{coil}. When the 3/1 RMP is increased to a critical value at approximately 0.39 s, $b_r^{n=1}$ shows a clear variation deviating from the linear increase, i.e. a decrease for this case with $\Delta\phi = 210°$. In addition, the plasma rotation around $q = 3$ RS (yellow line in figure 5(b)) changed towards the co-current direction, which is similar to the variation of 2/1 RMP penetration.

In figure 5(c), 3/1 mode penetration causes few changes in the ECE signals around the core and sawtooth behavior. The ECE signal around $q = 3$ RS shows a different tendency when 3/1 mode penetration occurs. The electron temperature T_e will decrease when an edge 3/1 island is excited [31]. Sometimes, the decrease can be observed in the ECE signal around $q = 3$ RS. This depends on the phase relation between the 3/1 locked island and the ECE location. Figure 5(d) shows the emission of carbon III (CIII) around the last closed

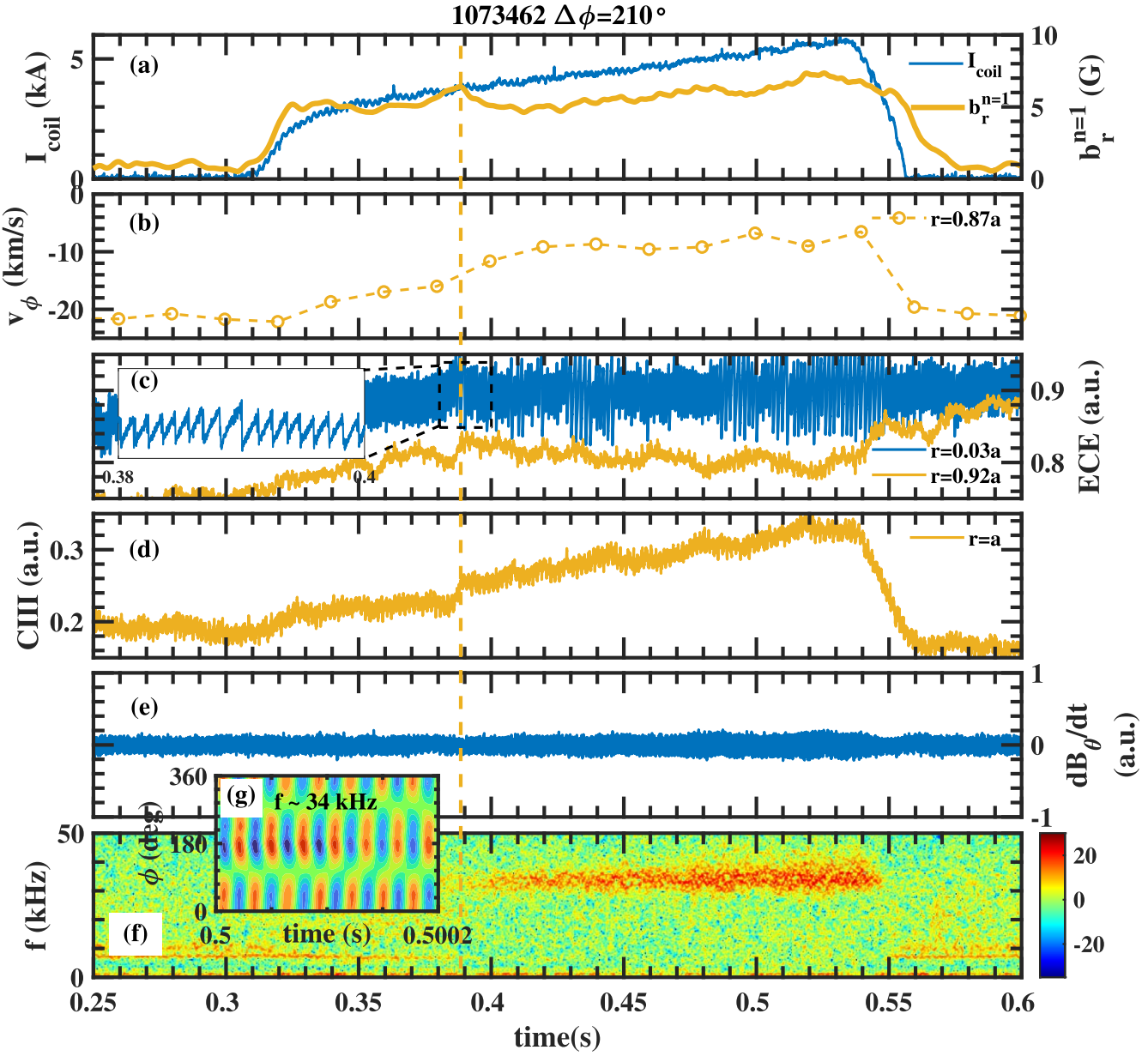

Figure 5. Time evolution of plasma parameters during 3/1 mode penetration discharge #1073462 with (a) RMP coil current and the measured $n = 1$ radial magnetic field, (b) toroidal rotation (co-I_p is the positive direction), (c) ECE signals around the core and the 3/1 RS, (d) carbon III emission around LCFS, (e) Mirnov signal, (f) spectrogram of the Mirnov signal, (g) the contour plot of filtered Mirnov signals measured by toroidal Mirnov probes.

flux surface (LCFS). The sudden increase in the CIII emission indicates a stronger interaction between the plasma and the limiters, which can support the formation of the edge 3/1 locked island.

Similar to the appearance of the 2/1 m-BAE, a 3/1 m-BAE is also observed from the time–frequency spectrum (figure 5(f)) at around 34 kHz and has a standing wave structure (figure 5(g)), indicating the formation of a 3/1 locked island. Therefore, the appearance of a 3/1 m-BAE can be used as an indicator for rapid confirmation of 3/1 mode penetration on J-TEXT. After the removal of the RMP field, there is no clear signature of the unlocking of a 3/1 island, which is different from the unlocking of a 2/1 island. The absence of 3/1 island unlocking might be related to the stability of the 3/1 island and that the 3/1 island decays very fast before it spins up to a few kHz.

Again, the thresholds of 3/1 mode penetration are shown by the full symbols in figure 6 for various RMP spectra, i.e. blue circles for $\Delta\phi$ =180°, red squares for $\Delta\phi = 225°$, yellow diamonds for $\Delta\phi = 270°$. For $\Delta\phi = 270°$, 3/1 RMP succeeds in achieving 3/1 mode penetration in all discharges. The thresholds of 3/1 mode penetration also have a non-monotonic dependence on density, which is similar to the 2/1 case shown in figure 4. Further studies will be needed to reveal the cause of this dependence. For $\Delta\phi = 180°$, 3/1 mode penetration is achieved with $n_e < 1.7 \times 10^{19} m^{-3}$, and

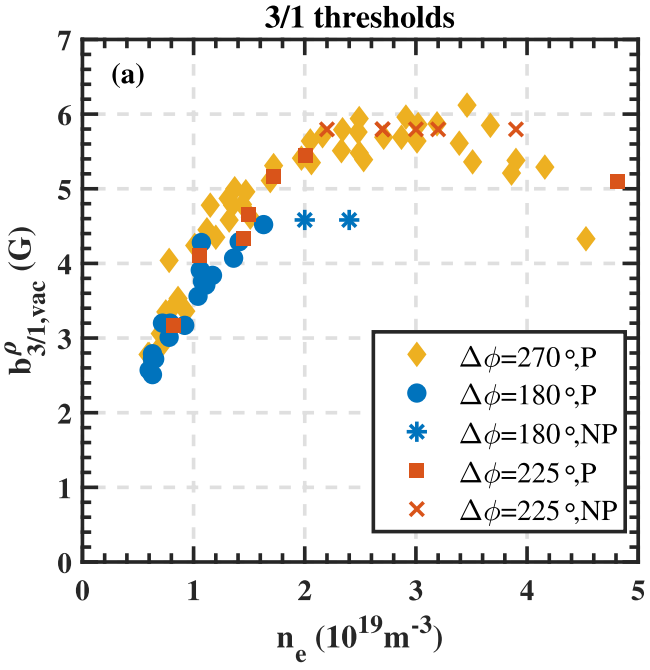

Figure 6. $3/1$ mode penetration thresholds obtained at various electron densities for three $\Delta\phi$ cases. The yellow diamonds (♦) represent thresholds with $\Delta\phi = 270°$. The blue squares (●) and blue stars (*) represent the thresholds and no penetration cases with $\Delta\phi = 180°$. The red squares (■) and crosses (×) are data with $\Delta\phi = 225°$.

the threshold increase is almost the same as the case of $\Delta\phi = 270°$. At higher n_e, the maximal $3/1$ RMP field with $\Delta\phi = 180°$ is below the mode penetration threshold, and the corresponding data are marked by blue stars in figure 6. For $\Delta\phi = 225°$, the maximal $3/1$ RMP field is larger and $3/1$ RMP penetration can be achieved at $n_e < 2.0 \times 10^{19}\,\mathrm{m}^{-3}$. Above $2.0 \times 10^{19}\,\mathrm{m}^{-3}$, no penetration is obtained for $\Delta\phi = 225°$ except a higher density discharge ($4.8 \times 10^{19}\,\mathrm{m}^{-3}$), although the available $3/1$ RMP amplitude is at the same level of threshold for the $\Delta\phi = 270°$. For the higher density ($4.8 \times 10^{19}\,\mathrm{m}^{-3}$), successful penetration with $\Delta\phi = 225°$ also supports that the $3/1$ RMP penetration threshold non-monotonically depends on the density. These features of the $3/1$ thresholds at various RMP spectra indicate that the vacuum $3/1$ RMP at the $q = 3$ RS ($b^{\rho}_{3/1,\mathrm{vac}}$) can describe the $3/1$ RMP penetration threshold with pretty good accuracy and that the single mode response ($3/1$) dominates during the penetration process in these situations.

3.3. Measurement of the intrinsic error fields

To evaluate the effect of the IEF on the mode penetration threshold, both $2/1$ and $3/1$ IEFs were measured by the 'compass scan' technique [24], as shown in figure 7. The data in figure 7(a) come from four discharges with the same plasma parameters and $\Delta\phi = 0°$. The amplitude of the $2/1$ IEF is $b^{\rho}_{2/1} = 0.64$ G and the toroidal phase is approximately 354°. Figure 7(b) shows that the amplitude of the $3/1$ IEF is $b^{\rho}_{3/1} = 0.27$ G and the toroidal phase is approximately 255°. Both $2/1$ and $3/1$ IEFs are much smaller than the mode penetration thresholds, so that the $2/1$ and $3/1$ IEFs can be ignored.

4. Multiple mode penetrations and their effect on the threshold

Before the major disruption induced by locked modes, it is generally assumed and observed that several LMs emerge due to the penetration of external RMP fields or IEFs [47, 48]. Those locked islands are likely to form subsequently. However, there has been little study on the thresholds of the latter formed island. Previous experiments on J-TEXT also show the $2/1$ mode penetration following $3/1$ locked island formation [31, 37], with limited poloidal spectra of the external RMP field. In this work, the ratio between $2/1$ and $3/1$ RMP fields can be varied flexibly with various $\Delta\phi$. This provides a good opportunity for studying the penetration of multiple modes.

With a flexible poloidal spectrum, the successive penetrations of the $3/1$ RMP followed by the $2/1$ RMP have been observed with $\Delta\phi \in [240°, 330°]$, as already summarized in table 1. Figure 8 displays a typical example of such a case with $\Delta\phi = 270°$, with the RMP amplitudes being $1.17\,\mathrm{G\,kA^{-1}}$ and $0.77\,\mathrm{G\ kA^{-1}}$ for $3/1$ and $2/1$ components, respectively. With the ramp-up of I_{coil}, $3/1$ mode penetration appears at 0.381 s (yellow vertical dashed line), as observed from the change in the $b_r^{n=1}$ signal (red line in figure 8(a)) and the 31 kHz m-BAE (figure 8(f)). After the formation of $3/1$ LM, the RMP is further ramped and $2/1$ mode penetration is clearly identified at 0.458 s (red vertical dashed line), as seen by the sudden increase in $b_r^{n=1}$, the disappearance of sawtooth oscillations and the variation of toroidal rotation towards co-I_p direction. Those features are more or less similar to the case with only a $2/1$ locked island. However, the m-BAE behaviors are different, i.e. mode frequency (figure 8(f)) increases from 31 to 44 kHz and the strength becomes weaker after $2/1$ mode penetration.

At $\Delta\phi = 270°$, $3/1$ mode penetration always appears first; the corresponding thresholds have already been displayed in figure 6. With the distinct identification of subsequent $2/1$ mode penetration, the $2/1$ thresholds can be measured with a pre-formed $3/1$ locked island, as shown by the yellow diamonds in figure 9. These $2/1$ thresholds increase with n_e, and when $n_e > 1.5 \times 10^{19}\,\mathrm{m}^{-3}$, no $2/1$ mode penetration is observed even with maximal RMP amplitude, as marked by the yellow crosses. A significant feature is revealed by comparing to the $2/1$ thresholds with $\Delta\phi = 0°$ (red full squares), i.e. the case with only $2/1$ mode penetration. The thresholds of $2/1$ mode penetration in $\Delta\phi = 270°$ are significantly lower than those in $\Delta\phi = 0°$ in the available density range ($<1.5 \times 10^{19}\ \mathrm{m}^{-3}$). This indicates that the pre-existing $3/1$ locked mode could significantly reduce the $2/1$ mode penetration threshold.

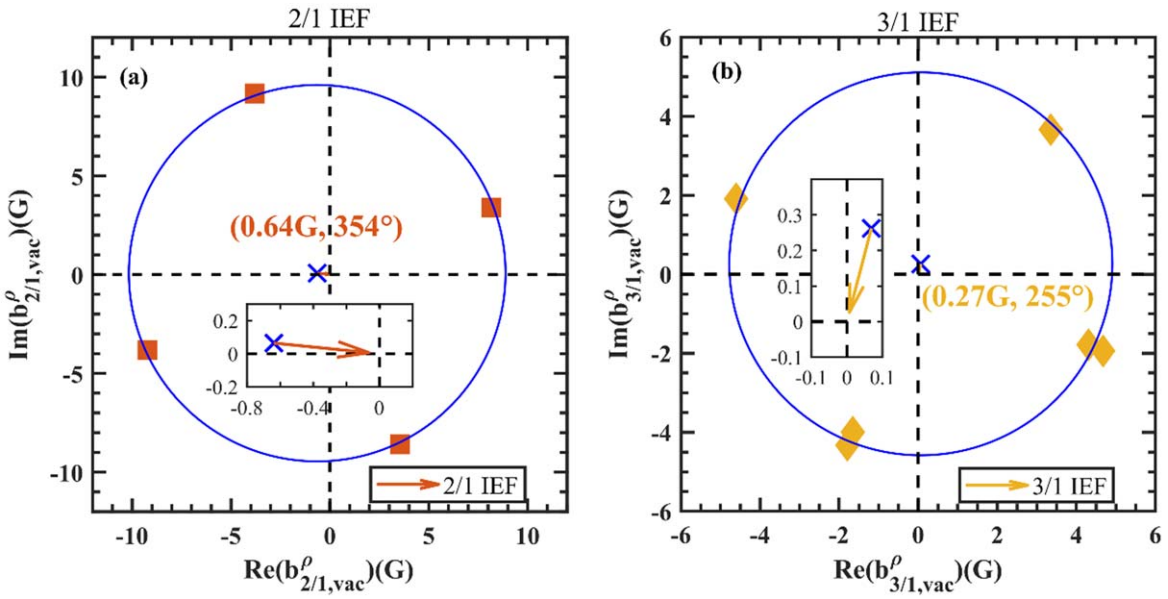

Figure 7. Intrinsic error fields measured by 'compass scan' technology. (a) The red squares (■) are 2/1 penetration thresholds for different discharges and the blue cross is the fitted center of the thresholds. The red arrow represents the final evaluated 2/1 intrinsic error field. (b) The yellow diamonds (♦) are 3/1 penetration thresholds for different discharges and the blue cross is the fitted center of the thresholds. The red arrow represents the final evaluated 3/1 intrinsic error field.

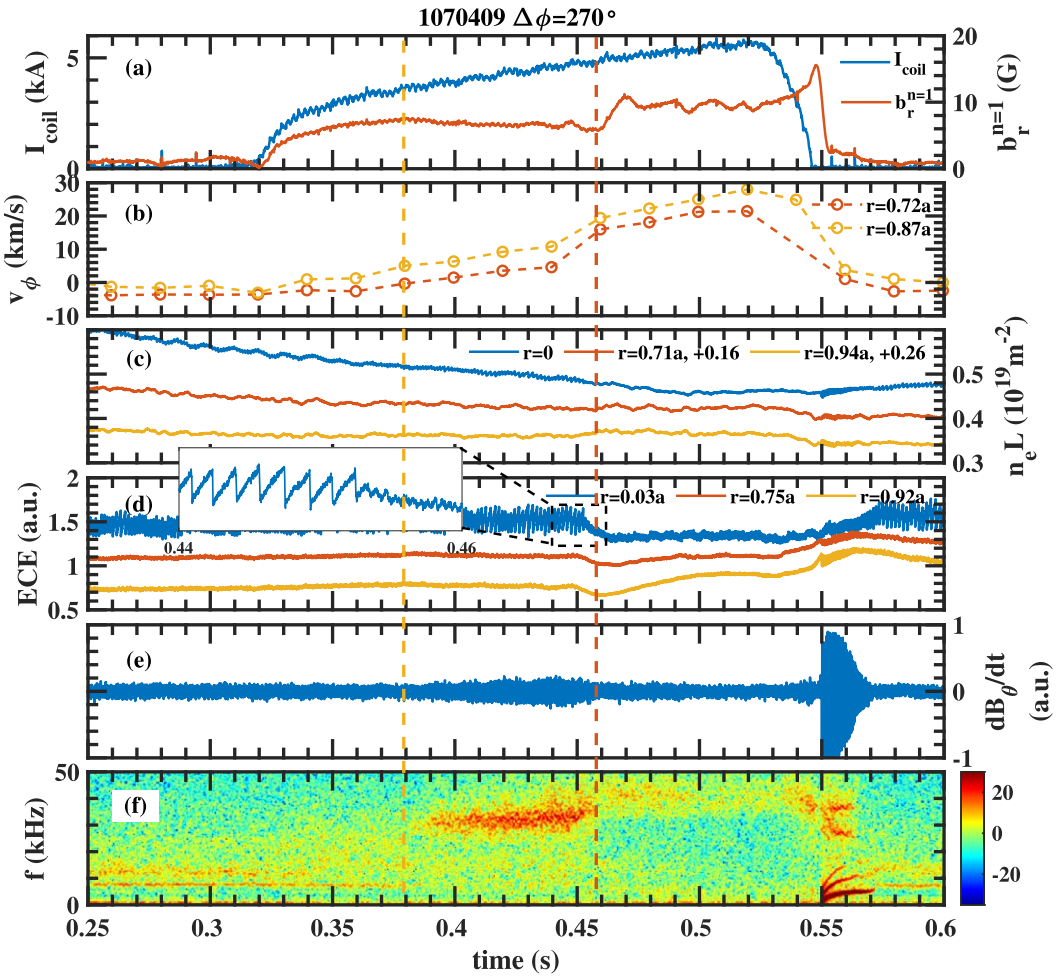

Figure 8. Time evolution of plasma parameters during multiple mode penetrations discharge #1070409. The moments of mode penetrations are marked by the yellow (3/1) and red (2/1) dashed vertical lines.

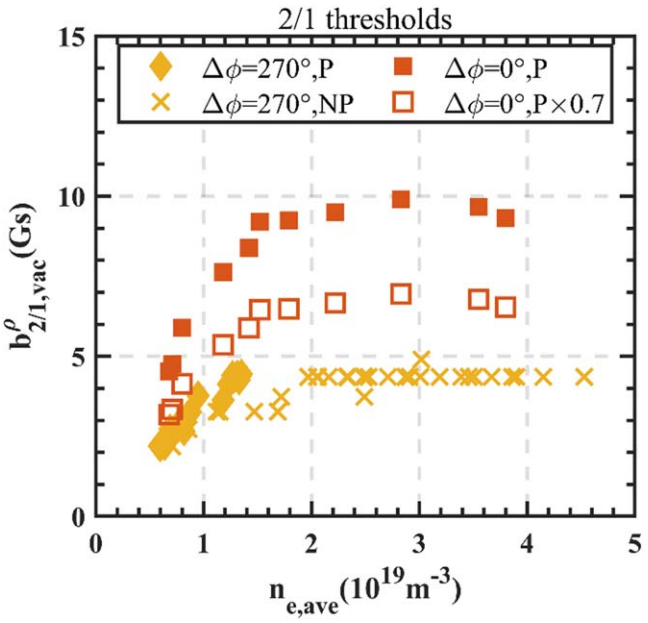

Figure 9. $2/1$ mode penetration thresholds obtained at various electron densities for two $\Delta\phi$ cases. The yellow diamonds (♦) represent the $2/1$ thresholds where $2/1$ mode penetration occurred after $3/1$ mode penetration with $\Delta\phi = 270°$. The yellow crosses (×) are the maximum values of the $2/1$ vacuum resonant field amplitude on the rational surface without $2/1$ mode penetration. The solid red squares (■) represent the $2/1$ thresholds with $\Delta\phi = 0°$ for which only one mode penetration occurred during discharges. The open red squares (□) have values which are 70% of the solid red squares.

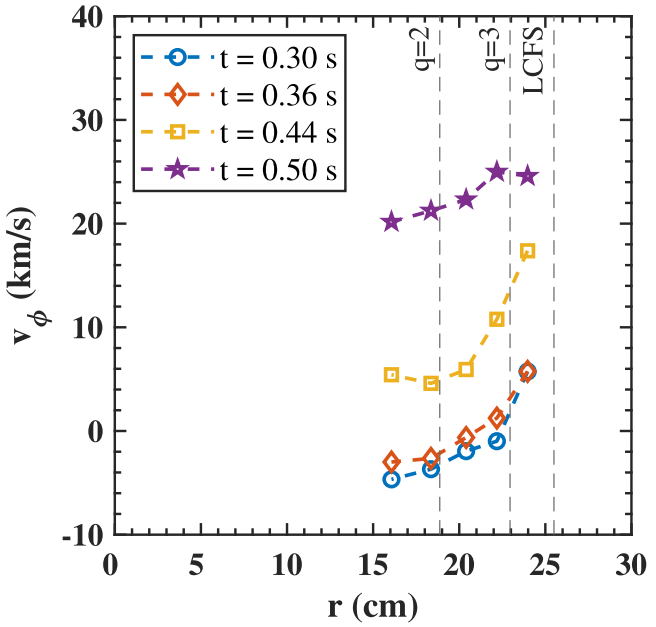

Figure 10. Toroidal rotation (co-I_p is the positive direction) profiles during multiple mode penetration in discharge #1070409.

5. Discussion

The reduction of the $2/1$ mode penetration threshold due to an edge locked island is important for the suppression of ELMs by using RMPs. During the ELM suppression the locked islands are believed to form at the pedestal top [9, 11]. According to the observations in this work, such pedestal top islands might significantly reduce the penetration thresholds at the inner rational surfaces and hence lead to the risk of exciting core locked islands. It is hence important to understanding why the $2/1$ threshold can be significantly reduced by a pre-existing $3/1$ locked island.

From a previous study on J-TEXT [32], plasma rotation is found to be the key factor in the mode penetration threshold. Plasma rotation profiles at different times for #1070409 are shown in figure 9: 0.3 s, 0.36 s, 0.44 s and 0.5 s are the times before RMP is applied, the linear response stage, during $3/1$ locked island and after $2/1$ mode penetration, respectively. The rotation profile during the linear response is almost the same as the profile without RMP. The rotation profile changes to the co-current direction when a $3/1$ locked island exists. The profile increases to a higher level after $2/1$ mode penetration. Therefore, the reduction in the $2/1$ mode penetration thresholds with a pre-existing $3/1$ locked island is thought to be related to the changes in the rotation profile induced by the $3/1$ locked island.

The effect of rotation variation is simply evaluated based on previous work. The scaling law of the $2/1$ mode penetration threshold on MHD frequency is $b_{r,2/1} \propto f_0^{1.04}$ [32]. The MHD frequency is estimated from the measured plasma rotation by the experimental relationship as $f_0 = 0.3V_\phi + 7.5$ [44]. Due to a lack of sufficient rotation data for all densities, the variation ratio of $V_\phi(q = 2)$ after $3/1$ mode penetration is assumed to be the same as for discharge #1070409 (figure 10). In discharge #1070409, the ratio of $V_\phi(q = 2)$ before and after $3/1$ mode penetration is $\frac{f_0'}{f_0} = 0.71$. According to the scaling law, such reduction will lead to a 30% decrease in the $2/1$ mode penetration threshold. $b^{\rho}_{2/1,th}$ at $\Delta\phi = 0°$ is multiplied by 70% and then displayed by the open squares in figure 10. These modified $2/1$ mode penetration thresholds, which take the rotation effect into account, are closer to but still higher than the thresholds of $\Delta\phi = 270°$. This indicates that the rotation variations due to the $3/1$ locked island only make a partial contribution to the reduction of the $2/1$ threshold. Other effects such as the magnetic perturbation from the $3/1$ locked island via toroidal coupling might also contribute.

6. Summary and outlook

In summary, the recent upgrade of the RMP coil connection on J-TEXT has enabled the study of the spectrum effects on RMP penetration. The poloidal spectrum is controlled by the coil phase differences $\Delta\phi$ in the experiment. Two kinds of effects on RMP penetration are found to be related to the poloidal spectrum. First, $\Delta\phi$ decides the type of RMP penetration, i.e. $2/1$ RMP penetration, $3/1$ RMP penetration or successive penetrations of $3/1$ RMP followed by the

2/1 RMP, as shown in table 1. Second, the RMP penetration thresholds are not consistent in all of the RMP spectra. For cases with penetration of only one RMP component, the penetration thresholds measured by the corresponding resonant component are close for various $\Delta\phi$. But for the cases with successive penetrations of 3/1 RMP followed by 2/1 RMP, the 2/1 RMP penetration threshold is significantly reduced. The reduction of the 2/1 RMP penetration threshold should be partly attributed to the variation in plasma rotation around $q = 2$ RS caused by the 3/1 locked mode. In addition, the non-monotonic dependence of 3/1 mode penetration thresholds on density is observed on J-TEXT for the first time. This point provides confidence for the formation of an edge island in high-density operation for island divertor configuration.

Although, the mode penetration thresholds can be well described by the vacuum RMP components for cases with only one penetration in this work, the plasma response has been demonstrated to play a crucial role [16, 17, 24]. Next we plan to study the spectral effects will be studied in consideration of the plasma response. The plasma responses on the basis of the MARS-F code [49] are under research and further results are on the way.

Acknowledgments

This work was supported by the National Magnetic Confinement Fusion Energy R & D Program of China (Nos. 2019YFE03010004, 2018YFE0309100), the National Key R & D Program of China (No. 2017YFE0301100) and National Natural Science Foundation of China (Nos. 11905078, 12075096 and 51821005).

ORCID iDs

Yangbo LI (李杨波) https://orcid.org/0000-0002-7635-2905
Abba Alhaji BALA https://orcid.org/0000-0002-2330-0749
Yunfeng LIANG (梁云峰) https://orcid.org/0000-0002-9483-6911

References

[1] Scoville J T *et al* 1991 *Nucl. Fusion* **31** 875
[2] Hender T C *et al* 1992 *Nucl. Fusion* **32** 2091
[3] Snipes J A *et al* 1988 *Nucl. Fusion* **28** 1085
[4] Garofalo A M *et al* 2000 *Nucl. Fusion* **40** 1491
[5] Evens T E *et al* 2004 *Phys. Rev. Lett.* **92** 235003
[6] Evens T E *et al* 2006 *Nat. Phys.* **2** 419
[7] Liang Y *et al* 2007 *Phys. Rev. Lett.* **98** 265004
[8] Tetsuya S and Takaya H 1979 *Phys. Fluids* **22** 1189
[9] Nazikian R *et al* 2015 *Phys. Rev. Lett.* **114** 105002
[10] Sun Y *et al* 2016 *Phys. Rev. Lett.* **117** 115001
[11] Hu Q *et al* 2020 *Phys. Rev. Lett.* **125** 045001
[12] Buttery R J *et al* 1999 *Nucl. Fusion* **39** 1827
[13] Boozer A H 2011 *Fusion Sci. Technol.* **59** 561
[14] Callen J D 2011 *Nucl. Fusion* **51** 094026
[15] Strait E J 2015 *Phys. Plasmas* **22** 021803
[16] Park J K *et al* 2007 *Phys. Rev. Lett.* **99** 195003
[17] Park J K *et al* 2008 *Nucl. Fusion* **48** 045006
[18] Reimerdes H *et al* 2009 *Nucl. Fusion* **49** 115001
[19] Paz-Soldan C *et al* 2015 *Phys. Rev. Lett.* **114** 105001
[20] Park J K *et al* 2018 *Nat. Phys.* **14** 1223
[21] Park J K *et al* 2021 *Phys. Rev. Lett.* **126** 125001
[22] Logan N C *et al* 2021 *Nucl. Fusion* **61** 076010
[23] Scoville J T and La Haye R J 2003 *Nucl. Fusion* **43** 250
[24] Wang H H *et al* 2016 *Nucl. Fusion* **56** 066011
[25] Cole A J *et al* 2007 *Phys. Rev. Lett.* **99** 065001
[26] Yang S M *et al* 2019 *Phys. Rev. Lett.* **123** 095001
[27] Ren J *et al* 2021 *Nucl. Fusion* **61** 056007
[28] Liang Y *et al* 2019 *Nucl. Fusion* **59** 112016
[29] Hu Q *et al* 2013 *Phys. Plasmas* **20** 092502
[30] Wang N *et al* 2014 *Nucl. Fusion* **54** 064014
[31] Hu Q *et al* 2016 *Nucl. Fusion* **56** 092009
[32] Huang Z *et al* 2020 *Nucl. Fusion* **60** 064003
[33] Wang N *et al* 2022 *Nucl. Fusion* **62** 042016
[34] Rao B *et al* 2014 *Fusion Eng. Des.* **89** 378
[35] Wang N *et al* 2022 *Rev. Modern Plasma Phys.* **6** 26
[36] Ren Z *et al* 2022 *Plasma Sci. Technol* Doi:10.1088/2058-6272/aca45f
[37] Liu L Z *et al* 2019 *Nucl. Fusion* **59** 126022
[38] Chen J *et al* 2014 *Rev. Sci. Instrum.* **85** 11D303
[39] Yang Z J *et al* 2012 *Rev. Sci. Instrum.* **83** 10E313
[40] Cheng Z F *et al* 2013 *Rev. Sci. Instrum.* **84** 073508
[41] Han D L *et al* 2021 *Plasma Sci. Technol.* **23** 055104
[42] Wang Y H *et al* 2022 *Plasma Sci. Technol.* **24** 064001
[43] Liu L Z *et al* 2015 *Plasma Phys. Control. Fusion* **57** 065007
[44] Yan W *et al* 2018 *Plasma Phys. Control. Fusion* **60** 035007
[45] Buratti P *et al* 2005 *Nucl. Fusion* **45** 1446
[46] Chen W *et al* 2011 *Nucl. Fusion* **51** 063010
[47] Du X D *et al* 2019 *Phys. Plasmas* **26** 042505
[48] Hu Q *et al* 2019 *Nucl. Fusion* **59** 016005
[49] Liu Y Q *et al* 2010 *Phys. Plasmas* **17** 122502